

# A Novel Systemic siDR6 Delivery System Based on DP7-C for the Treatment of Metastatic Lung Cancer

Hongyou Zhou\*, Rui Zhang\*, Ke Men , Lin Tang, Yusi Wang, Li Yang

Department of Biotherapy, Cancer Center and State Key Laboratory of Biotherapy, West China Hospital, Sichuan University, Chengdu, 610041, People's Republic of China

\*These authors contributed equally to this work

Correspondence: Rui Zhang; Li Yang, Email 526773225@qq.com; yl.tracy73@gmail.com

**Background:** The treatment of metastatic lung cancer, a common complication of many primary cancers, has historically been a significant clinical challenge. Once lung metastasis occurs, patients' survival is often significantly shortened. Therefore, prevention and treatment of lung metastases is an important aspect of cancer treatment. In this study, a simple, low-toxicity, cholesterol-modified cationic cell-penetrating peptide DP7 (DP7-C), in combination with siDR6 was used for intravenous administration for the treatment of lung metastases.

**Methods:** Initially, clinical databases were analyzed to determine the expression levels of death receptor 6 (DR6) in metastatic tumors and the correlation between DR6 expression and patient survival times. The DP7-C/siDR6 micelles were prepared by a self-assembly method. By cultivating 293T, B16F10 and LL2 cells, the in vitro experiments were performed to assess the transfection efficiency, safety and anti-cancer ability of DP7-C/siDR6, while its targeting efficiency and prevention of lungs were investigated by mouse experiments. Furthermore, the therapeutic efficacy of DP7-C/siDR6 was demonstrated in the LL2 model of lung cancer in situ, the B16F10 model of artificial lung metastasis, and the 4T1 model of spontaneous lung metastasis.

**Results:** The clinical data analysis revealed that DR6 was highly expressed in the majority of metastatic tumors and that patients with high DR6 expression exhibited significantly shorter survival times. The DP7-C/siDR6 showed high transfection efficiency, and it could inhibit tumor cell growth by suppressing the STAT3 signaling pathway. Subsequent mouse experiments demonstrated that intravenous administration of DP7-C/siDR6 resulted in efficient lung targeting. The inhibition of DR6 expression on lung endothelial cells was found to prevent metastasis-induced primary necrosis of lung endothelial cells, thereby preventing tumor metastasis. And the DP7-C/siDR6 treatment showed excellent therapeutic efficacy in the tumor models.

**Conclusion:** The systemic delivery of DP7-C micelles carrying siDR6 provide an alternative therapeutic strategy to halt cancer lung metastasis.

**Keywords:** DP7-C, siDR6, gene therapy, delivery system, metastatic cancer

## Introduction

It has been reported that more than 90% of cancer-related deaths are associated with metastasis.<sup>1-3</sup> Metastasis may occur at any stage of the disease, including in multiple cancers such as melanoma, breast cancer, lung cancer, and liver cancer.<sup>4-6</sup> Primary cancer cells typically metastasize to the lung, liver, brain, and bone. The lung has emerged as one of the most common metastatic organs for tumor cells due to its rich capillary network and low blood flow pressure.<sup>7,8</sup> Given the challenges inherent in the treatment of lung metastasis, approximately 30% of patients with cancer die from this complication.<sup>9</sup> While conventional treatments such as surgery, resection, chemotherapy, and radiotherapy exert a therapeutic effect to some extent, the therapeutic benefit of these treatments is unsatisfactory for the majority of

patients, and the drug resistance and toxic effects cannot be ignored.<sup>10–12</sup> Consequently, the objective of developing an effective and minimally invasive strategy to prevent lung metastasis represents a significant clinical aspiration.

Tumor cells primarily disseminate to other tissues via the circulatory system.<sup>13</sup> Thus, the successful passage of tumor cells through the endothelial barrier represents a critical factor in the formation of metastasis.<sup>14–16</sup> Consequently, necroptosis of endothelial cells has been identified as an important pathogenesis of tumor metastasis, and blocking the necroptosis pathway represents a potential strategy for the prevention of tumor metastasis.<sup>17,18</sup> DR6 belongs to the superfamily of tumor necrosis factor receptors and is also known as tumor necrosis factor receptor superfamily 21 (TNFRSF21).<sup>19–22</sup> It is expressed in mouse endothelial cells and is abnormally expressed in some tumor cell lines. The ligand of DR6 is amyloid precursor protein (APP), which is widely expressed in various tumor cells.<sup>23,24</sup> Studies have demonstrated that the activation of DR6 by APP is a prerequisite for endothelial cell necroptosis. And knockout of DR6 in mice (using an anti-DR6 antibody) has been shown to protect endothelial cells from necroptosis and tumor metastasis by inhibiting the phosphorylation of the pseudokinase mixed lineage kinase domain-like (MLKL).<sup>25</sup> Furthermore, there are also studies found that inhibiting the expression of DR6 in tumor cells could suppress tumor growth through the IL-6/STAT3 pathway.<sup>19</sup> Consequently, the targeting of DR6 may represent a novel approach to the prevention or treatment of metastasis.

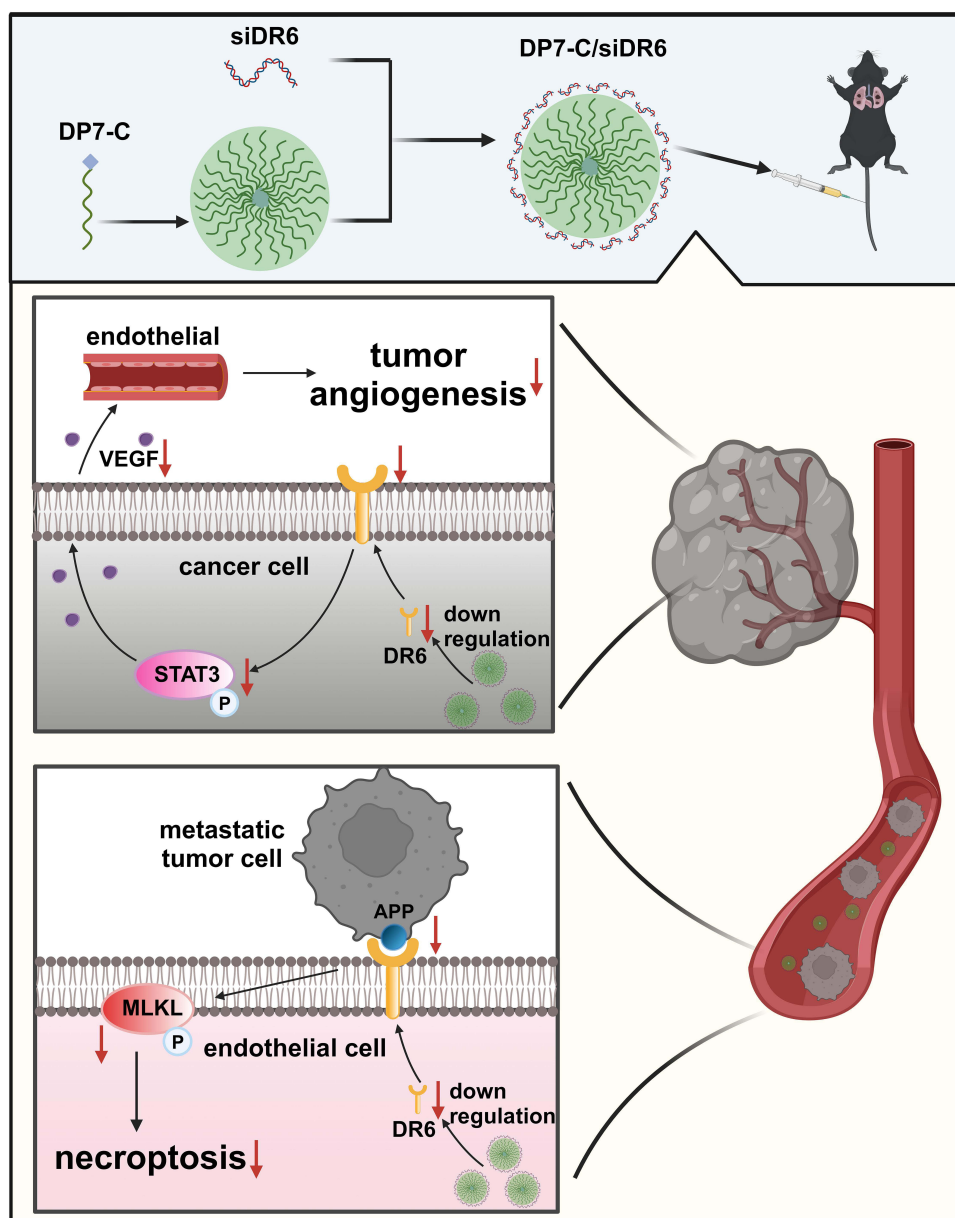
A multitude of studies have utilized siRNA for the treatment of diseases due to its high efficiency in silencing protein expression at the post-transcriptional level.<sup>26–28</sup> Furthermore, since siRNA exerts its gene silencing effects exclusively in the cytoplasm, which minimizes the risk of host gene mutations, siRNA treatment has an exceptional safety profile.<sup>29</sup> Conversely, our previous study demonstrated that cholesterol-modified DP7-C, derived from cationic cell-penetrating peptide DP7 (VQWRIRVAVIRK), could effectively and safely deliver antigen peptides and regulate the immune system by recruiting monocytes.<sup>30,31</sup> As nonviral vectors, cationic cell-penetrating peptides have been demonstrated to deliver siRNA effectively and safely *in vitro* and *in vivo*.<sup>32–34</sup> Moreover, in comparison to other conventional drug delivery systems, the intravenous route has been demonstrated to effectively deliver therapeutic agents to the site of lung diseases and to increase the drug concentration to a therapeutic level in the lung.<sup>35</sup>

Consequently, in this study, DP7-C was employed as a transport carrier to facilitate the intravenous delivery of siDR6 to metastatic lesions in the lungs (Scheme 1). The initial findings demonstrated that DP7-C exhibited optimal siRNA transfection efficacy and minimal cytotoxicity, which were comparable to those of other frequently utilized nonviral vectors. *In vitro* experiments demonstrated that DP7-C/siDR6 could inhibit tumor growth through the IL-6/STAT3 pathway. Subsequently, the mouse experiment demonstrated that the DP7-C/siDR6 intravenous delivery system exhibited excellent pulmonary targeting and successfully protected endothelial cells in the lung from necroptosis by inhibiting the expression of DR6. Finally, the efficacy of the systemic administration of DP7-C/siDR6 in the treatment of cancer lung metastases was demonstrated in three *in vivo* models of lung cancer: the LL2 model of lung cancer *in situ*, the B16F10 model of artificial lung metastasis, and the 4T1 model of spontaneous lung metastasis. In conclusion, this study provides a novel and highly effective gene therapy strategy for metastatic lung cancer, namely a therapy targeting lung metastasis-related genes.

## Materials and Methods

### Cells and Animals

The Roswell Park Memorial Institute (RPMI) 1640 medium, containing 100 units/mL streptomycin and penicillin (PS) and 10% fetal bovine serum (FBS), was utilized to cultivate the 4T1 cells (American Type Culture Collection, Manassas, VA, USA). Dulbecco's Modified Eagle Medium (DMEM) containing 100 units/mL streptomycin and penicillin (PS) and 10% fetal bovine serum (FBS) was utilized to cultivate B16F10, LL2 and 293T cells (American Type Culture Collection, Manassas, VA, USA). All cells were maintained in a cell incubator with 5% CO<sub>2</sub> at 37°C. RPMI 1640 medium, DMEM medium, fetal bovine serum (FBS), and penicillin-streptomycin (PS) were all purchased from Thermo Fisher Scientific. Female six- to eight-week-old C57BL/6J mice and BALB/c mice were obtained from Beijing Vital River Laboratory Animal Technology Co., Ltd. All animal procedures were approved and controlled by the Institutional Animal Care and



**Scheme 1** Schematic illustration of DP7-C/siDR6 as a general strategy for cancer immunotherapy. The DP7-C/siRNA complex could be formed by simple incubation. After intravenous injection, DP7-C/siDR6 can efficiently knock down DR6 expression in tumor cells to inhibit the expression of angiogenesis related cytokines, and thus inhibit tumor growth. Besides, DP7-C/siDR6 can also knock down DR6 expression in endothelial cells to inhibit the necroptosis of endothelial cells induced by the interaction of APP and DR6.

Treatment Committee of Sichuan University and conducted in accordance with the Animal Care and Use Guidelines of Sichuan University.

### Characterization of DP7-C Micelles and the DP7-C/siRNA Complex

The DP7-C powder was synthesized by GL Biochem Co., Ltd. (Shanghai, China) with a purity of greater than 98%. The HPLC and MS results for DP7-C is shown in [supplementary figures 1](#) and [2](#). The negative control siRNA (siNC), siDR6, Cy5-siNC, and FAM-siNC were procured from GenePharma Co., Ltd. (Shanghai, China). The DP7-C micelles were prepared via a self-assembly method. In brief, 5 mg of DP7-C powder was added directly to 1 mL of aqueous solution and incubated at 50°C for 20 minutes. The prepared DP7-C micelles were subsequently lyophilized or stored at 4°C. The mean particle size and zeta potential of DP7-C (60 µg/mL) and DP7-C (60 µg/mL)/siRNA (12 µg/mL) were determined

using a Malvern ZetaSizer Nano-ZS Zen3600 (Malvern Instruments, Ltd., Worcestershire, UK). All results are presented as the mean of three test runs. The morphology of DP7-C and DP7-C/siRNA was observed by transmission electron microscopy (TEM) (JSM-7500F; FEI).

## In Vitro Transfection Efficiency

A total of  $1 \times 10^5$  B16F10, LL2, or 4T1 cells were inoculated into 24-well plates. DP7-C (1.2  $\mu\text{g}$ )/FAM-siRNA (0.24  $\mu\text{g}$ ), PEI25K (0.24  $\mu\text{g}$ )/FAM-siRNA (0.24  $\mu\text{g}$ ), and Lipo2000 (0.48  $\mu\text{g}$ )/FAM-siRNA (0.24  $\mu\text{g}$ ) were incubated in serum-free medium for 10 minutes before being added to the above cells cultured in serum-free medium. Following a four-hour incubation period, the serum-free medium was replaced with medium containing 10% serum to continue the incubation process for 20 hours. Subsequently, the fluorescence was observed under a fluorescence microscope (Zeiss, USA) and photographed. Finally, the cells were collected and resuspended for flow cytometry analysis of the percentage of FAM-positive cells (BD Biosciences, USA).

## Cytotoxicity Assays

The cytotoxicity of DP7-C to 293T cells was compared with that of Lipo2000 and PEI25K (Sigma) using the 3-(4,5-Dimethylthiazol-2-yl)-2,5-Diphenyltetrazolium Bromide Assay (MTT assay) (KeyGen BioTECH, China). In brief, 293T cells were seeded in 96-well plates at a density of  $1 \times 10^4$  cells per well. Subsequently, the cells were subjected to a series of transfection reagents at concentrations of 5, 10, 20, 40, 60, 80, 120, 150, and 200  $\mu\text{g}/\text{mL}$  for 72 hours. Following this, 10  $\mu\text{L}$  of MTT solution was added to each well and incubated at  $37^\circ\text{C}$  for 4 hours. Subsequently, the culture supernatant was discarded and 100  $\mu\text{L}$  of DMSO was added. The SpectraMax M5 Microtiter Plate Luminometer (Molecular Devices, USA) was then employed to quantify the optical density (OD) value at 570 nm.

## Endosomal Escape Assay

The endosomal escape assays were conducted in accordance with the previously described methodology.<sup>36</sup> Briefly, B16F10 ( $1 \times 10^5$  cells/well) were seeded in a 24-well plate containing cell climbing films for 24 h. Next, DP7-C (1.2  $\mu\text{g}$ )/FAM-siRNA (0.24  $\mu\text{g}$ ) was added to the cells for 24 h. For endosomal staining, the cells were fixed with 4% paraformaldehyde for 20 min at room temperature and washed three times with PBS for 5 min each. For early endosome staining, cells were treated with 0.1% Triton X-100 for 20 minutes at room temperature and washed three times with PBS for 5 minutes each. Subsequently, an antibody specific for the early endosome marker EEA1 (Invitrogen, USA) (1:100) was added to the sample for 2 hours at room temperature and thoroughly washed five times for 5 minutes each with PBS. Subsequently, the PE-labeled secondary antibody (BD, USA) (1:100) was added to the sample for an additional 40 minutes at room temperature, after which three washes with PBS were performed for 5 minutes each. For late endosome staining, a PE-labeled anti-LAMP1 antibody (BD, USA) (1:100) was added to the sample for 40 minutes at  $4^\circ\text{C}$ , after which three washes with PBS were performed for 5 minutes each. Subsequently, all samples were stained with DAPI (Beyotime Biotechnology, China) for 40 minutes at  $4^\circ\text{C}$ . Finally, all the cell climbing films were acquired for confocal analysis.

## In Vivo Distribution of Intravenous Administration

To examine the in vivo distribution of DP7-C/siRNA injected intravenously, we injected DP7-C (60  $\mu\text{g}$ )/Cy5-siRNA (12  $\mu\text{g}$ ) complexes intravenously into mice. Twenty-four hours later, the major organs of the mice were excised and imaged ex vivo using the PerkinElmer IVIS Lumina III.

## Bioinformatic Analysis

The expression level of DR6 was verified in GEPIA2 (<http://gepia2.cancer-pku.cn/>) and TNMplot platform (<https://tnmplot.com/>). The main functions provided by GEPIA2 include gene expression analysis, gene correlation analysis, survival analysis, similar gene prediction, and dimensionality reduction analysis. And the TNMplot platform is a web tool for the comparison of gene expression in normal, tumor, and metastatic tissues. Besides, the relationship between DR6 expression level and prognosis was analyzed via the PanCanSurvPlot (<https://smuonco.shinyapps.io/>

[PanCanSurvPlot/](#)) and GEPIA2. All samples included in the prognosis analysis were classified into low-expression and high-expression groups by the median expression of DR6. The log-rank significance test was employed as the statistical method for analyzing the relationship between DR6 expression level and the survival rate of patients, with a 95% confidence interval (CI). Furthermore, we verified the positive correlation between DR6 expression and tumor stage in UALCAN (<http://ualcan.path.uab.edu/index.html/>).

## RNA Isolation and Real-Time PCR

The siDR6 sequence utilized in this study was 5'-UUUACACUUCAUCACACUGGAAGGC-3'. In the in vitro study, logarithmically growing B16F10 cells ( $5 \times 10^5$ ) were transfected with DP7-C (6  $\mu$ g)/siDR6 (1.2  $\mu$ g) complexes for 24 h. Thereafter, the cells were collected and lysed with TRIzol reagent (Life Technologies). In the in vivo study, C57BL/6J mice were injected with saline, DP7-C (60  $\mu$ g), DP7-C (60  $\mu$ g)/siNC (12  $\mu$ g), or DP7-C (60  $\mu$ g)/siDR6 (12  $\mu$ g) via the tail vein, once every 24 h for three consecutive times. Twenty-four hours after the final injection, mouse lung tissues were collected, frozen in liquid nitrogen, ground, and lysed by the addition of TRIzol reagent. Total RNA was extracted from the TRIzol lysate using a phenol-chloroform extraction method. Subsequently, the RNA was reverse transcribed using the Takara kit (Takara, China). Reverse transcription-polymerase chain reaction (RT-PCR) was conducted using SYBR Green, and levels were quantified over 40 cycles using an iQ5 optical system (Bio-Rad, Hercules, CA, USA). The primers for real-time quantitative PCR were synthesized by Chengdu Kengke Biotechnology Co. The primer sequences for mouse DR6 were 5'-TGTGCGGAAGAAGGGGACAG-3' (upstream) and 5'-AGAGAAGGTGGGGTTTGTGC-3' (downstream). The primer sequences for  $\beta$ -actin were 5'-TGTGCTGTCCCTGTATGCCTCT-3' and 5'-GGAACCGTCGTTGCCAATAGT-3'. The primer sequences for mouse IL-6 were 5'-CAGAAGGAGTGGCTAAGGACCA-3' upstream and 5'-ACGCACTAGGTTTGCCGAGTAG-3' downstream, while the primer sequences for mouse PDGF- $\alpha$  were 5'-TCTCTGCTGCTACCTGCGTCTG-3' and 5'-GGAAGTTGGCGTTGGTGCATC-3'.

## Western Blot Analysis

In the in vitro study, logarithmically growing B16F10 cells ( $5 \times 10^5$ ) were transfected with DP7-C (6  $\mu$ g)/siDR6 (1.2  $\mu$ g) complexes for 24 h. Thereafter, total protein extracted from B16F10 cells was subjected to sodium dodecyl sulfate polyacrylamide gel electrophoresis. The proteins were probed with antibodies against DR6 (BioVision, Milpitas, CA, USA), STAT3, p-STAT3 (Cell Signaling Technology, Danvers, MA, USA), VEGF-D (Cell Signaling Technology, Danvers, MA, USA), GAPDH (Cell Signaling Technology, Danvers, MA, USA) and then with an appropriate horseradish peroxidase (HRP)-conjugated secondary antibody (Cell Signaling Technology, Danvers, MA, USA). A chemiluminescence system (Millipore, MA, USA) was employed to visualize the target proteins.

## Plate Clone Formation Assay

Inoculate the cell suspension of B16F10 cells (1000 cells/mL) into a 6-well plate. After 24 hours, the cells were treated with PBS, DP7-C (6  $\mu$ g), DP7-C (6  $\mu$ g)/siNC (1.2  $\mu$ g), or DP7-C (6  $\mu$ g)/siDR6 (1.2  $\mu$ g) at 37 °C for 10 days until visible clones appeared. Subsequently, the cells were fixed with paraformaldehyde for 15 minutes and stained with crystal violet for another 15 minutes. Finally, the number of clones should be counted and the clone formation rate calculated. This is done by dividing the number of clones in the experimental group by the number of clones in the PBS group and multiplying the result by 100%.

## In Vivo Inhibition of Endothelial Cells Necroptosis

Saline, DP7-C (60  $\mu$ g), DP7-C (60  $\mu$ g)/siNC (12  $\mu$ g), or DP7-C (60  $\mu$ g)/siDR6 (12  $\mu$ g) was administered intravenously to female C57BL/6J mice for three consecutive days. On the fourth day, mice were inoculated with B16F10 cells ( $2.5 \times 10^5$ ) via the tail vein. All mice were euthanized on day 5. Lung tissues were collected from the mice and immediately snap frozen in liquid nitrogen. They were then embedded in optimal cutting temperature compound (OCT; Titanium Tek, Sakura USA, Torrance, CA, USA) at  $-18^\circ\text{C}$ . The embedded tissues were then sectioned at 4  $\mu$ m thickness using a cryostat (CM 1900, Leica, Germany). For immunofluorescence staining, 5% BSA was added to the tissues and incubated for 20 minutes at room temperature to block nonspecific binding. Then an antibody specific for phospho-

MLKL (S345) (1:50; Huaan Biotechnology, China) or CD31 (1:500; Abcam, Nanjing, China) was added and incubated at 4°C. After overnight incubation, goat anti-rabbit IgG H&L (Alexa Fluor® 488) (Abcam, Nanjing, China) was incubated for 30 minutes at room temperature. The sections were then incubated with EthD-III (MKBio, China) for 30 minutes at room temperature. The nuclei were then stained with DAPI (Beyotime Biotechnology, China) for 20 minutes at room temperature. The sections were imaged with a Zeiss microscope.

## In Vivo Transfection Efficiency

In vivo studies were conducted by administering DP7-C (60 µg)/Cy5-siRNA (12 µg), Lipo2000 (24 µg)/Cy5-siRNA (12 µg), or PEI25K (12 µg)/Cy5-siRNA (12 µg) complexes intravenously into mice. After 2 and 24 hours, the lung tissue of the mice was excised and frozen in liquid nitrogen. It was then stored in optimal cutting temperature compound (OCT; Titanium Tek, Sakura USA, Torrance, CA, USA) at -18 °C. Frozen lung specimens were sectioned at 6 µm using a cryostat (CM 1900, Leica, Germany) and mounted on glass slides. Subsequently, the cell nuclei were stained with DAPI (Beyotime Biotechnology, China) at 4 degrees Celsius for 40 minutes. Finally, a fluorescence microscope was employed for photography.

## Cell Viability Assay

The impact of interfering with tumor cell DR6 on cell viability was evaluated using the MTT assay (KeyGen BioTECH, China). In brief, B16F10 cells were inoculated in 96-well plates at a density of  $1 \times 10^4$  cells per well. Twenty-four hours later, the cells were treated with PBS, DP7-C (0.3 µg), DP7-C (0.3 µg)/siNC (0.06 µg), or DP7-C (0.3 µg)/siDR6 (0.06 µg). Each group was set up with three replicates. After 48 hours, 10 µL of MTT solution was added to each well and incubated at 37°C. Following a four-hour incubation period, the culture solution was removed and 100 µL of dimethyl sulfoxide was added to the cells. The optical density (OD) value at 570 nm was then determined using a SpectraMax M5 microplate photometer (Molecular Devices, USA).

## In Vivo Inhibition of Tumor Growth and Metastasis

The initial objective was to ascertain whether the inhibition of DR6 could impede tumor growth and metastasis. To this end, a therapeutic artificial lung metastasis model was established. First, female C57BL/6J mice were inoculated with B16F10 ( $2.5 \times 10^5$ ) or LL2 ( $3 \times 10^5$ ) cells via the tail vein. On the third day, mice were administered saline, DP7-C (60 µg), DP7-C (60 µg)/siNC (12 µg), or DP7-C (60 µg)/siDR6 (12 µg) via the tail vein, respectively, every two days for six times. On the third day following the final treatment, all mice were euthanized. Lung tissues were collected from the mice for photographic documentation, weighing, and the enumeration of lung nodules.

Subsequently, the objective was to ascertain whether interfering with DR6 on lung endothelial cells could prevent tumor metastasis. A saline solution, DP7-C (60 µg), DP7-C (60 µg)/siNC (12 µg), or DP7-C (60 µg)/siDR6 (12 µg) was administered intravenously to female C57BL/6J mice on three consecutive days. On the fourth day, the mice were inoculated with B16F10 cells ( $2.5 \times 10^5$ ) through the tail vein. All mice were euthanized on day 16. Lung tissue was collected from mice for photographic documentation and the enumeration of lung nodules.

Furthermore, we established a spontaneous lung metastasis model to validate the effect of interfering DR6 on tumor metastasis. In brief, female BALB/c mice were orthotopically inoculated with 4T1 ( $5 \times 10^5$ ) cells in the fourth mammary fat pad in the right lower abdomen. At approximately 50 cubic millimeters, the tumor size was reached, and the mice were treated every two days via the tail vein with saline, DP7-C (60 µg), DP7-C (60 µg)/siNC (12 µg), or DP7-C (60 µg)/siDR6 (12 µg) for a total of seven sessions. Tumor volume was recorded at two-day intervals. All mice were euthanized on the third day following the final treatment. Lung tissues were collected from the mice for photographic documentation, weighing, and the enumeration of lung nodules.

## In Vivo Safety Evaluation and Histological Analysis

After the mice were sacrificed, blood was collected for biochemical analysis, including analyses of aspartate transaminase (AST), alanine aminotransferase (ALT), creatinine (CREA) and UREA. The main organs were harvested and fixed immediately using 4% paraformaldehyde. They were then embedded in paraffin. Subsequently, the embedded tissue was

sectioned at a thickness of 4  $\mu\text{m}$ . For CD31 detection, following hydration, sections were treated with high pressure for antigen retrieval and then incubated with an endogenous peroxidase blocker (Zsfg-Bio, Beijing, China) for 10 minutes. Subsequently, an anti-CD31 antibody (1:500; Abcam, Nanjing, China) was added and incubated for one hour at room temperature. One hour later, the sections were incubated for 30 minutes with an appropriate HRP-conjugated secondary antibody (Zsfg-Bio). Finally, the positive signal was visualized with a DAB kit (Zsfg-bio), and the sections were stained with hematoxylin.

For immunofluorescence staining, the sections were subjected to high-pressure antigen retrieval after hydration. 5% BSA was then added to the tissues and incubated at room temperature for 20 min to block nonspecific binding. Antibodies specific for the surface markers Ly-6C, F4/80, CD4 and CD8 were then added and incubated at 4°C for 30 minutes. Antibodies recognizing the intracellular markers CD206 and IFN- $\gamma$  were added to a buffer that disrupted membranes and incubated at 4°C for 30 minutes. Subsequently, the cell nuclei were stained with DAPI for 30 minutes at 4°C. The sections were imaged using a Leica DMI microscope, and images were acquired using a Leica DFC camera with element software. Besides, the sections of the spontaneous lung metastasis model were used to assess the In vivo inhibition of endothelial cells necroptosis by DP7-C/siDR6. After antigen retrieval and blocking as before, antibody specific for phospho-MLKL (S345) (1:50; Huaan Biotechnology, China) was added and incubated at 4°C. After overnight incubation, Goat Anti-Rabbit IgG H&L (Alexa Fluor<sup>®</sup> 488) (Abcam, Nanjing, China) was incubated at room temperature for 30 min. And then the sections were incubated with EthD-III at room temperature for 30 min. Subsequently, the cell nuclei were stained with DAPI for 10 minutes at room temperature. The sections were imaged using a Zeiss microscope.

To assess the prevalence of apoptosis in each model, tumor tissue specimens were subjected to terminal deoxynucleotidyl transferase-mediated deoxyuridine triphosphate-biotin nick-end labeling (TUNEL) staining (Promega, Madison, WI, USA). A DM 2500 fluorescence microscope (Leica Microsystems CMS GmbH, Wetzlar, Germany) was employed for the observation and digitization of the sections. A total of five random fields at 200 $\times$  magnification was selected for the enumeration of apoptotic cells (TUNEL-positive). Finally, the main organs were examined by Mayer's hematoxylin-eosin (H&E) staining.

## Statistical Analysis

All the values in the present study are presented as the mean $\pm$ s.d. unless otherwise indicated in the Figure captions. One-way analysis of variance was used for multiple comparisons (ANOVA) when more than two groups were compared, followed by post hoc Tukey's multiple comparison test, and Student's *t*-test was used for two-group comparisons. All the statistical analyses were carried out with the GraphPad Prism software package (PRISM 9.0; GraphPad Prism Software). Statistical significance was set at a threshold of  $P < 0.05$ . Significant differences are denoted as follows: \* $P < 0.05$ , \*\* $P < 0.01$ , \*\*\*  $P < 0.001$ , and \*\*\*\*  $P < 0.0001$ .

## Results

### Characterization of DP7-C Micelles and Evaluation of Its Intracellular Behavior

In this study, DP7-C micelles were synthesized according to a self-assembly method, omitting the use of carriers, surfactants, or organic solvents. Consequently, the preparation method for DP7-C micelles was a convenient one. Positively charged DP7-C micelles adsorb negatively charged siRNA mainly through electrostatic action, thus allowing the DP7-C/siRNA complex to be formed by simple incubation (Figure 1a). Transmission electron microscopy (TEM) revealed that both DP7-C and DP7-C/siRNA exhibited a spherical structure in an aqueous solution (Figure 1b). The average particle size of DP7-C micelles was  $46.06 \pm 1.51$  nm, with a polydispersity index (PDI) of 0.176 and a zeta potential of  $47.72 \pm 0.27$  mV (Figure 1c and d). The average particle size of the DP7-C/siRNA complex was  $107.52 \pm 1.13$  nm with a polydispersity index (PDI) of 0.216 and a zeta potential of  $19.63 \pm 0.31$  mV (Figure 1c and d). These results are consistent with the diameter of the DP7-C/siRNA complexes observed by transmission electron microscopy (TEM). Moreover, carriers utilized for systemic delivery of siRNA should exhibit high siRNA transfection efficiency. Therefore, FAM-siRNA was employed to assess the transfection efficiency of DP7-C, Lipo2000, and PEI25K in B16F10,

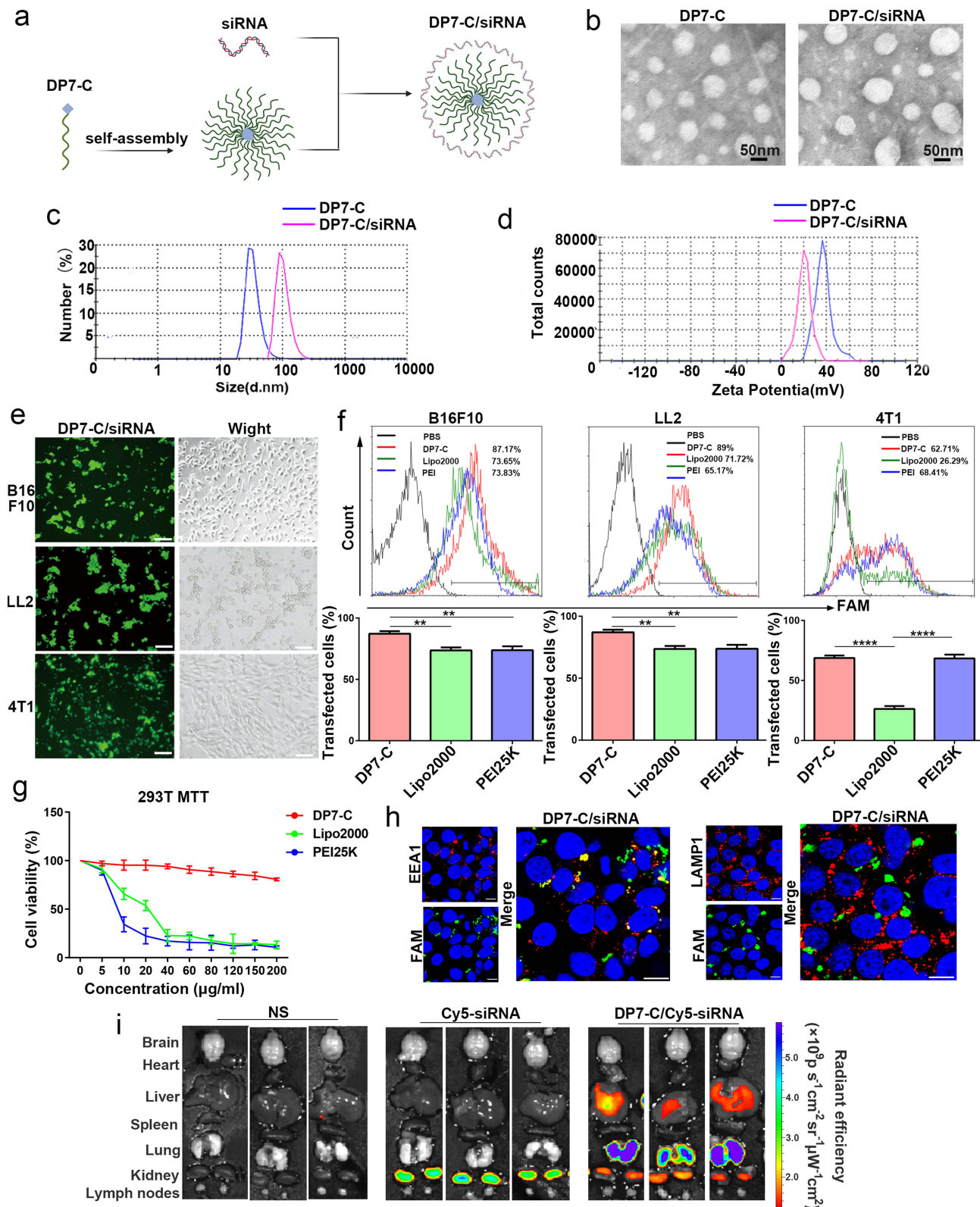


**Figure 1** Characterization of DP7-C and the DP7-C/siRNA complex. (a) Schematic representation of the complex formation of DP7-C and siRNA. (b) Transmission electron microscopy of the DP7-C and DP7-C/siRNA complex. (c) Particle sizes of DP7-C and the DP7-C/siRNA complex. (d) Zeta potentials of DP7-C and the DP7-C/siRNA complex. The transfection efficiency of FAM-siRNA delivery by DP7-C in B16F10, LL2 and 4T1 cells was analyzed by (e) fluorescence microscopy and (f) flow cytometry analysis. Scale bar, 50 μm. (g) MTT assay testing the toxicity of materials to 293T cells. (h) Colocalization of DP7-C/siRNA complexes with intracellular endosomes. Scale bar, 10 μm. (i) In vivo spectrum imaging system (IVIS) fluorescence imaging of isolated brain, heart, liver, spleen, lung, kidney and inguinal LNs from C57BL/6 mice after administration of Cy5-siRNA or DP7-C/Cy5-siRNA. All values presented in this figure are expressed as the mean ± s.d., unless otherwise indicated in the figure captions. Statistical analysis was performed using one-way ANOVA with Dunnett's multiple comparison test. \*\*P<0.01, \*\*\*\*P<0.0001.

LL2, and 4T1 cells. As illustrated in [Figure 1e](#) and [f](#), DP7-C demonstrated comparable or higher transfection efficiency than other reagents. In addition to high delivery efficiency, delivery carriers should also exhibit low cytotoxicity. Therefore, we evaluated the cytotoxicity of DP7-C and compared it with Lipo2000 and PEI25K. As shown in [Figure 1g](#), as the concentration increased, more than 80% of DP7-C-treated cells survived. However, less than 20% of cells survived after treatment with other transfection materials. The results demonstrated that the cytotoxicity of DP7-C was less than that of other cationic or liposomal transfection materials. Additionally, it was observed that carriers delivering siRNA into cells must escape from the endosome. Therefore, the localization of DP7-C/siRNA complexes in intracellular endosomes was assessed, and it was found that the complexes were not colocalized with late endosomes 24 h after transfection ([Figure 1h](#)). This indicates that the DP7-C/siRNA complexes escaped from late endosomes. Finally, the systemic distribution of siRNA delivered by DP7-C was assessed. As illustrated in [Figure 1i](#), in comparison to the Cy5-siRNA group, the DP7-C/siRNA group exhibited a notable increase in the fluorescence intensity of the lung and liver. Consequently, it was determined that DP7-C, as an siRNA delivery system, is capable of successfully delivering siRNA to the lung, exhibiting higher transfection efficiency and lower cytotoxicity than the commonly utilized siRNA delivery vectors Lipo2000 and PEI25K.

## Inhibition of DR6 Expression Has Been Demonstrated to Suppress Tumor Growth and to Inhibit Tumor-Induced Primary Necrosis of Lung Endothelial Cells

The Gene Expression Profiling Interactive Analysis (GEPIA) web tool enables the analysis of gene expression based on data from the Cancer Genome Atlas Program (TCGA) and the Genotype-Tissue Expression (GTEx) databases. The expression profile of DR6 was analyzed across all tumor samples and paired normal tissues using GEPIA2. The results demonstrate that DR6 is highly expressed in tumor tissues in comparison to normal tissues in the majority of cancer types, including lung adenocarcinoma (LUAD), lung squamous cell carcinoma (LUSC), and skin cutaneous melanoma (SKCM) ([Supplementary Figure 3a](#)). In addition, we examined the correlation between DR6 expression levels and cancer prognosis. As illustrated in [supplementary figure 3b](#) and [c](#), patients exhibiting low DR6 expression exhibited longer overall survival and disease-free survival compared to those exhibiting high DR6 expression. Besides, we employed PanCanSurvPlot, an online tool for conducting survival analysis, to investigate the relationship between DR6 expression and the prognosis of different cancers. The results indicate that patients with low DR6 expression exhibit a higher survival rate across a range of cancers such as lung cancer, lung adenocarcinoma and breast cancer ([Figure 2b](#), [Supplementary Figure 3d](#) and [e](#)). And the expression of DR6 in cancers based on individual cancer stages was investigated by UALCAN, the results exhibit positive correlation between DR6 expression and tumor grade in LUAD and LUSC ([Supplementary Figure 3f](#) and [g](#)). Furthermore, given the close relationship between DR6 and metastasis, we also compared the expression profile of DR6 in normal and metastatic tissues using the TNM plot. This revealed that DR6 was highly expressed in metastatic tissues compared to normal tissues in lung ([Figure 2c](#)).

DR6 is expressed in mouse B16F10 melanoma cells.<sup>19</sup> First, the expression of DR6 in B16F10 cells was evaluated following the knockdown of DR6 expression through the transfection of DP7-C/siDR6 complexes. As illustrated in [Figure 2](#), DR6 expression was diminished at both the mRNA and protein levels following treatment with DP7-C/siDR6 complexes for 24 hours ([Figure 2d](#) and [e](#), [supplementary figure 4](#)). As previously reported in the literature, DR6 can increase the expression of tumor angiogenesis-related cytokines by up-regulating the expression of IL-6 and the phosphorylation of downstream STAT3 ([Figure 2a](#)).<sup>19,37</sup> Therefore, we analyzed the protein levels of VEGF-D, STAT3, and p-STAT3 in B16F10 cells after DP7-C/siDR6 treatment by Western blot analysis. As illustrated in [Figure 2e](#), the quantity of p-STAT3 and VEGF-D was diminished in DP7-C/siDR6-transfected B16F10. Furthermore, the expression of IL-6 and PDGF- $\alpha$  in the B16F10 cells was quantified by quantitative polymerase chain reaction (qPCR). As illustrated in [Figure 2f](#) and [g](#), the levels of IL-6 and PDGF- $\alpha$  mRNA were significantly diminished in B16F10 cells with suppressed DR6 expression. STAT3 is intimately associated with tumor growth.<sup>38</sup> Consequently, the growth of DP7-C/siDR6-treated cells were evaluated through colony formation and MTT experiments. The results demonstrated that cell growth was inhibited following the knockdown of DR6 expression ([Figure 2h-j](#)). These findings indicated that

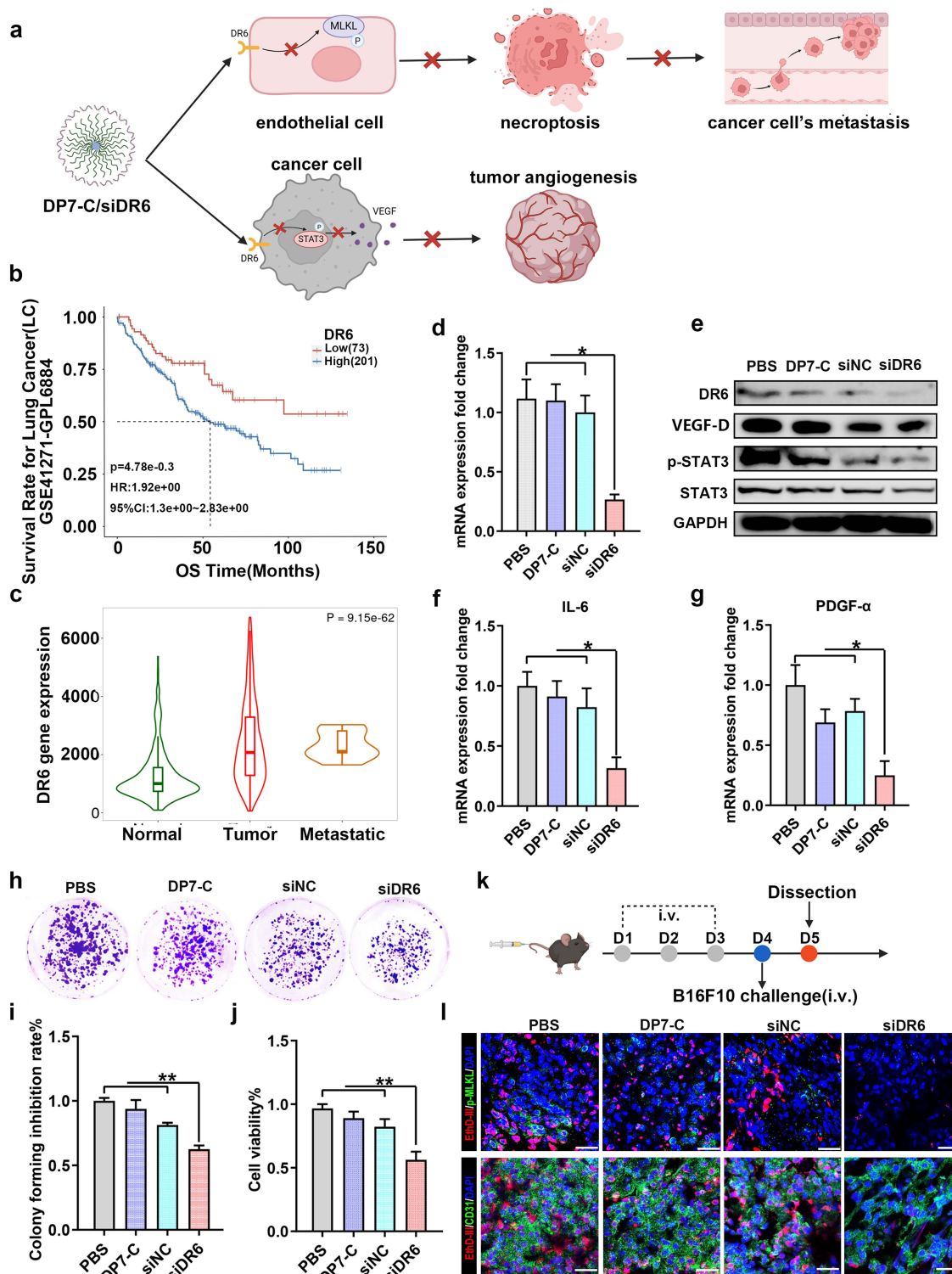


**Figure 2** A preliminary in vitro mechanistic study of interfering with DR6 to block tumor growth and metastasis. (a) Schematic representation of the mechanism of action of DP7-C/siDR6 complexes. (b) Survival correlation analysis on DR6 expression levels in lung cancer specimens. (c) DR6 expression in normal, tumor and metastatic tissues. (d) Detection of DR6 mRNA expression after DP7-C-mediated transfection of siDR6 into B16F10 cells. (e) The protein expression levels of DR6, STAT3, p-STAT3 and VEGF-D after DP7-C-mediated transfection of siDR6 into B16F10 cells. (f) IL-6 and (g) PDGF-α mRNA expression after DP7-C-mediated transfection of siDR6 into B16F10 cells. (h-i) The inhibitory effect of the DP7-C/siDR6 complex was quantified by means of a clonogenic assay. The number of clones in each well was converted into an inhibition rate. (j) The inhibitory effect of the DP7-C/siDR6 complex was determined by an MTT assay. (k) Experimental design. (l) Necroptosis of endothelial cells in lungs were detected by EthD-III staining and immunofluorescence assays with antibody against CD31 and phospho (p)-MLKL. Scale bar, 20 μm. All values presented in this figure are expressed as the mean ± s.d., unless otherwise indicated in the figure captions. Statistical analysis was performed using one-way ANOVA with Dunnett's multiple comparison test. \*P< 0.05, \*\*P< 0.01.

DP7-C could deliver siDR6 into tumor cells *in vitro* and inhibit the growth of tumor cells by inhibiting the IL-6/STAT3 pathway.

To demonstrate whether siDR6 can inhibit tumor cells-induced necroptosis of lung endothelial cells *in vivo*, the lungs were examined by EthD-III staining and immunofluorescence assays with endothelial-specific antibody against CD31. EthD-III indicates necrotic cells with compromised membrane integrity. As illustrated in [Figure 2l](#), in comparison to other groups, the siDR6 group exhibited a significant decrease in endothelial cells necroptosis. Furthermore, as shown in [Figure 2l](#), the siDR6 group also exhibited a significant decrease in the phosphorylation of MLKL, indicating that siDR6 can inhibit tumor-induced necroptosis of lung endothelial cells through the inhibition of MLKL phosphorylation.

## Systemic Administration of DP7-C/siDR6 has Been Demonstrated to Inhibit Tumor Growth and Metastasis in Both Artificial Lung Metastasis Models and Spontaneous Lung Metastasis Model

To further verify the entry of DP7-C/siRNA complexes into cells following intravenous administration, frozen sections were evaluated. The results demonstrated that all DP7-C groups exhibited greater red fluorescence around the nucleus than other groups ([Figure 3a](#) and [b](#)), indicating that DP7-C exhibited superior intravenous delivery efficiency compared with Lipo2000 and PEI25K. To assess the antitumor efficacy of intravenous DP7-C/siDR6 delivery, we initially established B16F10 and LL2 artificial lung metastasis models to evaluate the therapeutic impact ([Figure 3c–h](#)). As illustrated, the administration of DP7-C/siDR6 complexes via the tail vein resulted in a notable suppression of B16F10 and LL2 tumor growth, as evidenced by a significant reduction in lung weight and the number of lung nodules in the DP7-C/siDR6 treatment group ([Figure 3d–f](#), [3i–k](#)). To further evaluate the potential of intravenous DP7-C/siDR6 delivery to affect tumor metastasis by inhibiting the expression of DR6 in pulmonary endothelial cells, we first injected DP7-C/siDR6 intravenously to interfere with DR6 in pulmonary endothelial cells and then injected B16F10 cells to observe their growth in the lungs ([Figure 4a](#)). The results demonstrated that intravenous injection of DP7-C/siDR6 complexes successfully disrupted DR6 expression in pulmonary epithelial cells ([Figure 4b](#)), which prevented B16F10 lung metastasis ([Figure 4c–e](#)). Finally, we established a 4T1 spontaneous lung metastasis model to evaluate the antitumor effect of intravenous DP7-C/siDR6 delivery ([Figure 5a](#)). The results demonstrated that *in situ* vaccination with 4T1 cells followed by intravenous administration of DP7-C/siDR6 complexes not only inhibited the growth of orthotopic tumors ([Figure 5b](#) and [c](#)), but also prevented lung metastasis, as evidenced by significant decreases in lung weight and lung nodule numbers in the DP7-C/siDR6 treatment group ([Figure 5d–f](#)).

It has been demonstrated that DR6 deficiency can influence tumor angiogenesis through the IL-6/STAT3 pathway.<sup>19</sup> Consequently, the impact of DP7-C/siDR6 on tumor angiogenesis was also evaluated. The analysis of tumor tissues by CD31 staining revealed a significant reduction in the density of blood vessels in the DP7-C/siDR6 group compared with that in the other groups ([Figures 3g](#), [3l](#), [4f](#) and [5g](#)). This suggests that DP7-C/siDR6 can inhibit tumor angiogenesis by reducing the expression of DR6. Furthermore, TUNEL staining demonstrated a higher prevalence of apoptotic cells in tumors in the DP7-C/siDR6-treated group compared to the other groups ([Figure 5h](#)). And as shown in [Figure 5i](#), the siDR6 group also exhibited a significant decrease in the necroptosis and the phosphorylation of MLKL, indicating that siDR6 can inhibit tumor-induced necroptosis in lungs through the inhibition of MLKL phosphorylation. These findings suggest that intravenous administration of DP7-C/siDR6 can suppress tumor metastasis, growth, and angiogenesis.

## DP7-C and DP7-C/siDR6 Administration Contributes to Immune Cell Recruitment Into the Tumor Microenvironment

Previous experiments have demonstrated that DP7-C has immunomodulatory effects, promoting the recruitment of immune cells into the tumor microenvironment and improving the suppressive tumor immune microenvironment.<sup>39</sup> To verify whether the tumor microenvironment was also improved after intravenous administration of DP7-C and in combination with siDR6, we examined immune cell infiltration in the tumor microenvironment of 4T1 tumors *in situ*. Immunofluorescence staining demonstrated that the number of infiltrating cells in the tumor microenvironment was increased in all DP7-C groups,

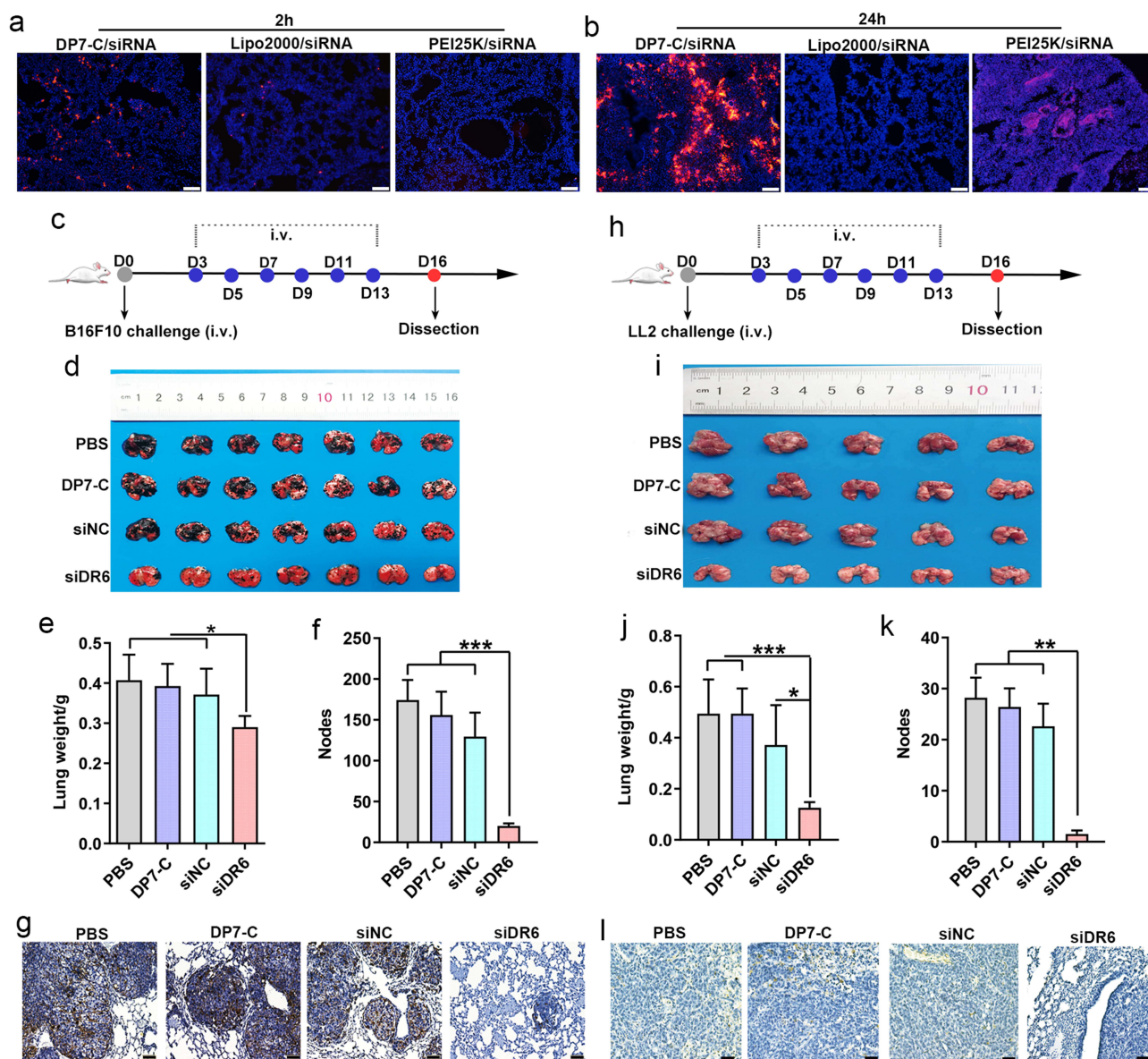


**Figure 3** Artificial lung metastasis tumor growth was inhibited by the DP7-C/siDR6 complex in vivo. At (a) 2 h or (b) 24 h post-intravenous injection of the different delivery vectors/siRNA complexes, the red fluorescence of cells was detected after frozen sectioning. (c) Experimental design. (d) Representative images for the B16F10 artificial lung metastasis model. (e) Lung weight of each group. (f) Number of tumor nodules of each group. (g) Vessels in tumor tissues were detected by CD31 staining. (h) Experimental design. (i) Representative images for the LL2 artificial lung metastasis model. (j) Lung weight of each group. (k) Number of tumor nodules of each group. (l) Vessels in tumor tissues were detected by CD31 staining. Scale bar, 200  $\mu$ m. All values presented in this figure are expressed as the mean  $\pm$  s.d., unless otherwise indicated in the figure captions. Statistical analysis was performed using one-way ANOVA with Dunnett's multiple comparison test. \* $P < 0.05$ , \*\* $P < 0.01$ , \*\*\* $P < 0.001$ .

including monocytes (Ly6C<sup>+</sup>), macrophages (F4/80<sup>+</sup>), and T-cells (CD4<sup>+</sup> T-cells, CD8<sup>+</sup> T-cells, and IFN- $\gamma$ -producing cells), whereas the number of M2-type macrophages (CD206<sup>+</sup>) in the tumor microenvironment was decreased (Figure 6). These findings suggest that DP7-C and DP7-C/siDR6, when administered intravenously, may also be capable of promoting immune cell recruitment into the tumor microenvironment and ameliorating the suppressive tumor immune microenvironment.

### Evaluation of the Safety of Intravenous DP7-C/siDR6 Administration

The evaluation of safety is a crucial metric for the assessment of the DP7-C/siDR6 drug delivery system. Consequently, we conducted a comprehensive evaluation of the safety of DP7-C/siDR6 systemic administration through the use of major organ staining. In a previous study, it was demonstrated that all mice survived when DP7-C was administered intravenously at doses up to 80 mg/kg. When DP7-C was administered intravenously at a dose up to 10 mg/kg, there

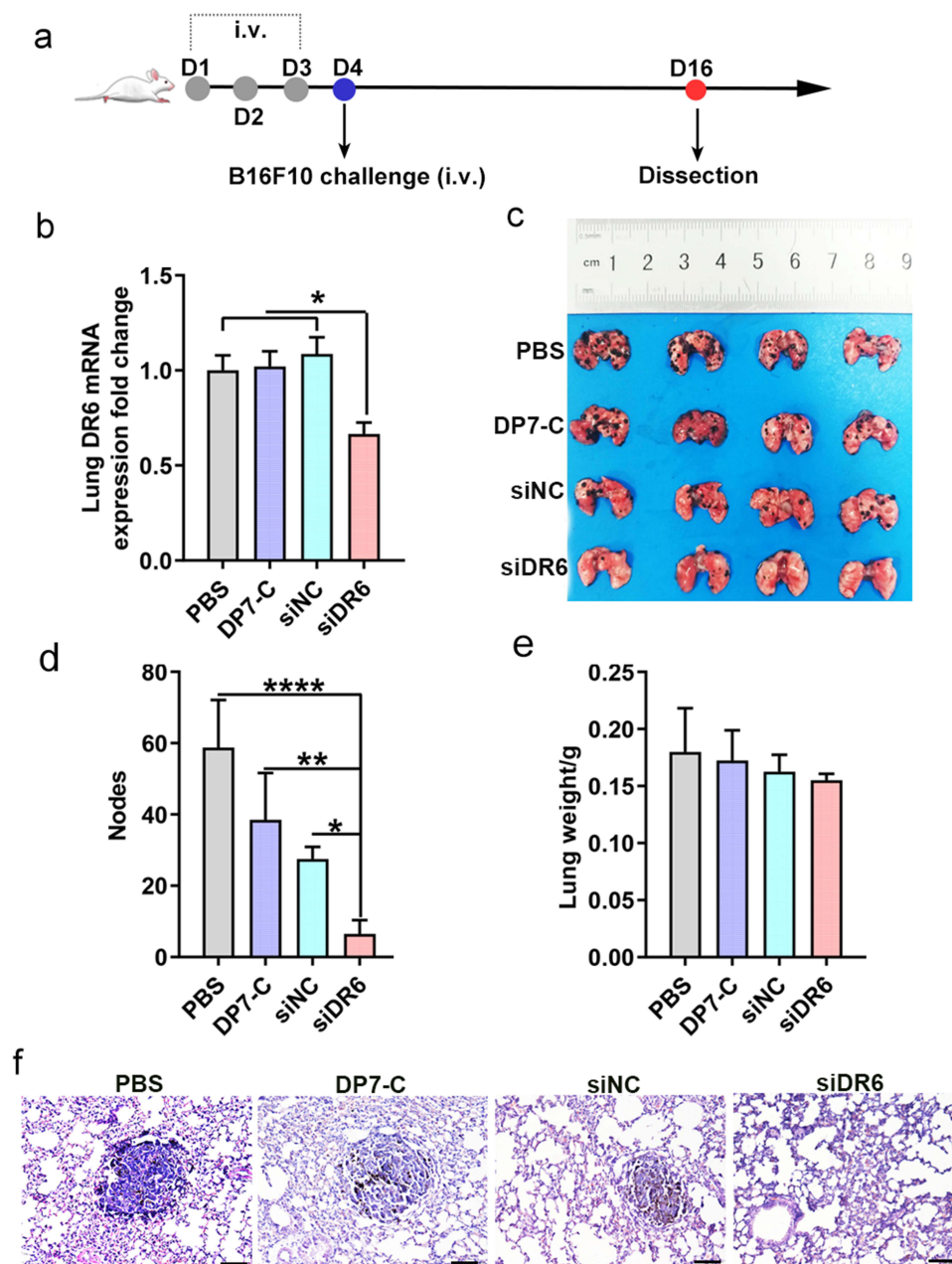


**Figure 4** The DP7-C/siDR6 complex inhibited tumor growth in the prophylactic artificial B16F10 lung metastasis model. (a) Experimental design. (b) Detection of DR6 interference efficiency in pulmonary endothelial cells at the mRNA level. (c) Representative images for the B16F10 preventive lung metastasis model of each group. (d) Number of tumor nodules of each group. (e) Lung weight of each group. (f) Vessels in tumor tissues were detected by CD31 staining. Scale bar, 50  $\mu$ m. All values presented in this figure are expressed as the mean  $\pm$  s.d., unless otherwise indicated in the figure captions. Statistical analysis was performed using one-way ANOVA with Dunnett's multiple comparison test. \* $P < 0.05$ , \*\* $P < 0.01$ , \*\*\*\* $P < 0.0001$ .

were no apparent abnormalities in the routine blood indices and blood biochemical indices of the mice, and no discernible toxic side effects were observed in the major organs.<sup>31</sup> This preliminary analysis suggests that intravenous administration of DP7-C is safe. In this experiment, despite multiple repeated administrations of DP7-C, the dose of DP7-C per injection was only 60  $\mu$ g, which was considerably lower than the previously verified safe dose. Histological examination of major organs from 4T1 spontaneous lung metastasis mice revealed that DP7-C administration did not result in any significant organ toxicity following multiple administrations (Figure 7). Furthermore, there was no significant difference in body weight among PBS, DP7-C, siNC and siDR6 groups (Supplementary figure 5a). And blood biochemical assays demonstrated that the parameters of liver (AST, ALT) and kidney (CREA, and UREA)

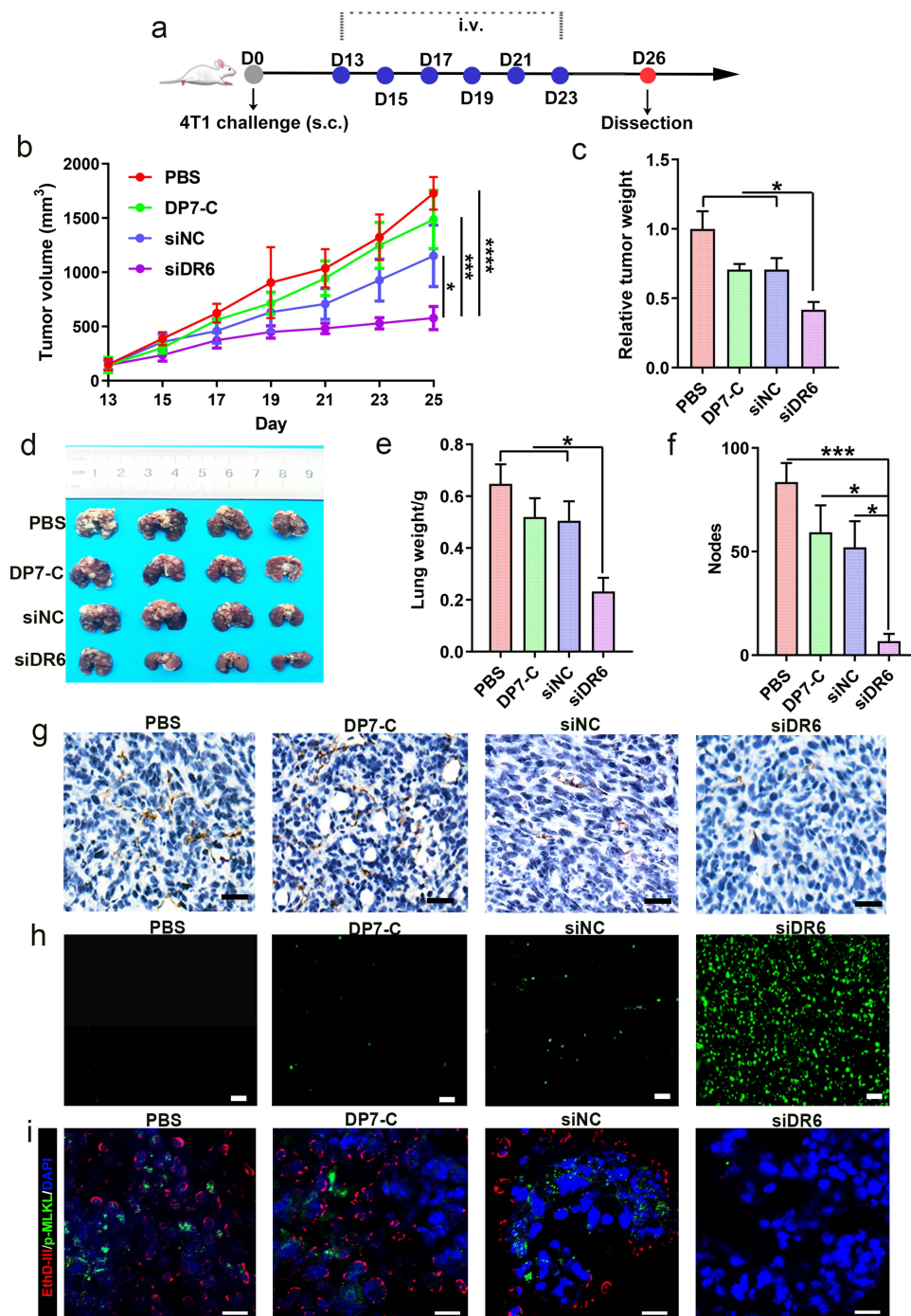


**Figure 5** The DP7-C/siDR6 complex demonstrated efficacy in inhibiting tumor growth in a spontaneous pulmonary metastasis model of 4T1 melanoma. (a) Experimental design. (b) Tumor growth curve of each group. (c) Tumor weight of each group. (d) Representative images of pulmonary metastases. (e) Lung weight of each group. (f) Number of tumor nodules of each group. (g) Vessels in tumor tissues were detected by CD31 staining. Scale bar, 50  $\mu$ m. (h) Apoptosis in tumor tissues were detected by TUNEL staining. Scale bar, 20  $\mu$ m. (i) Representative confocal images of lung sections stained with p-MLKL, EthD-III and DAPI. Scale bar, 20  $\mu$ m. All values presented in this figure are expressed as the mean  $\pm$  s.d., unless otherwise indicated in the figure captions. Statistical analysis was performed using one-way ANOVA with Dunnett's multiple comparison test. \* $P$  < 0.05, \*\*\* $P$  < 0.001, \*\*\*\* $P$  < 0.0001.

functions were not significantly impacted in DP7-C, siNC, siDR6 in comparison to the PBS control ([Supplementary figure 5b](#)). This preliminary observation suggests that intravenous DP7-C/siDR6 injections are safe under the conditions of the present experiment.

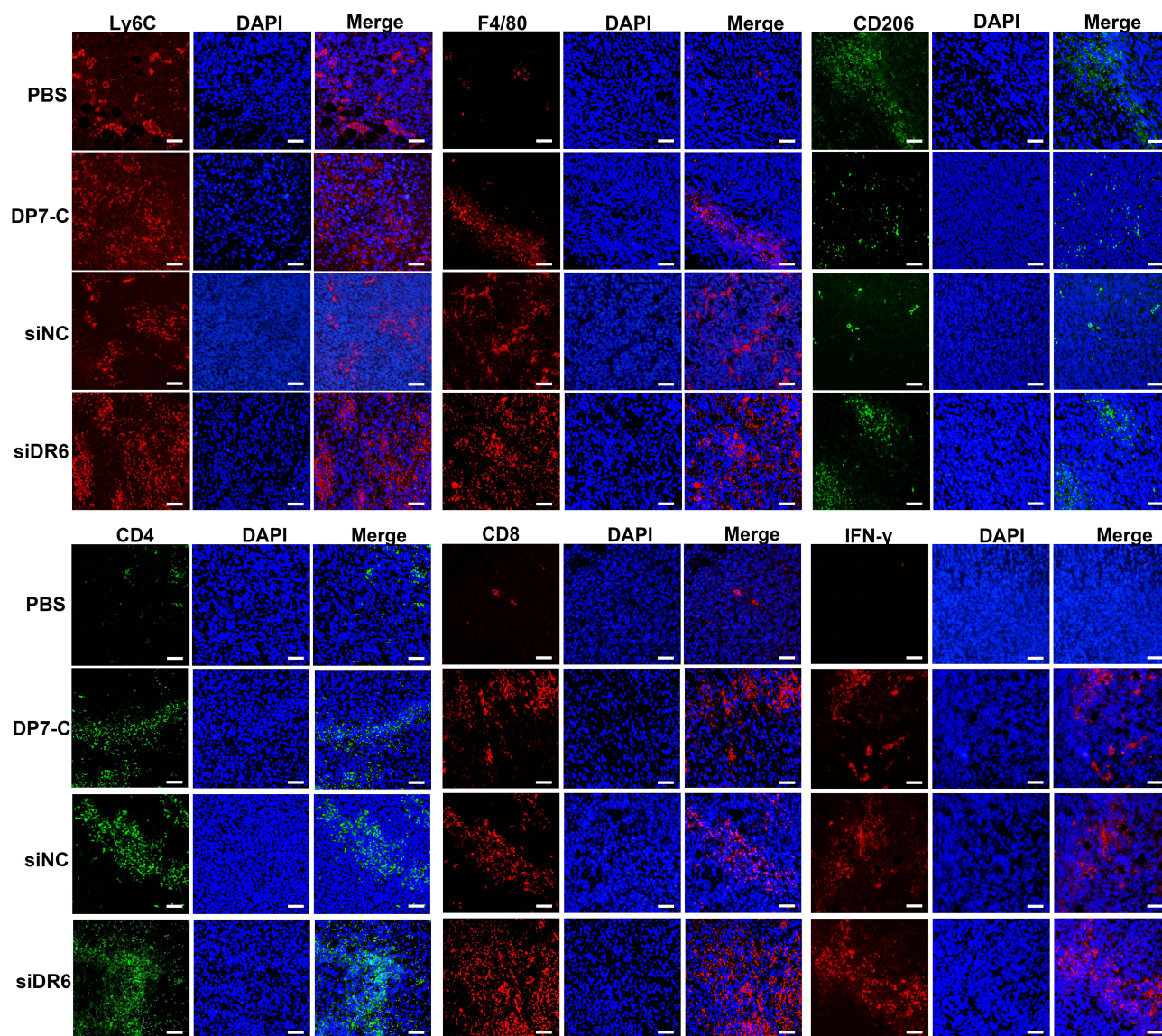


**Figure 6** Immunofluorescence analysis of subcutaneous 4T1 tumor tissue from each treatment group. Detection of monocytes, M2-type macrophages, CD4<sup>+</sup> T cells, CD8<sup>+</sup> T cells and IFN- $\gamma$ <sup>+</sup> T cells in the tumor microenvironment. Scale bar, 50  $\mu$ m.

## Discussion

The treatment of metastatic lung cancer, a common complication of many primary cancers, has historically been a significant clinical challenge.<sup>9</sup> While traditional treatments such as surgery, chemotherapy, and radiotherapy have the potential to prolong survival, they are often accompanied by high recurrence rates, strong side effects, and low quality of life.<sup>11</sup> Therefore, it is of paramount importance to explore new, highly effective treatments with low side effects. DP7-C micelles, a highly efficient drug delivery system, can carry siDR6 intravenously to reach metastatic lesions in the lungs, thereby enabling the delivery of a targeted therapy with a certain degree of precision. This targeting not only enhances the therapeutic efficacy, but also minimizes the damage to other tissues and reduces the side effects, thus providing a guarantee for its safety in clinical application. Therefore, DP7-C/siDR6 systemic drug delivery represents a novel option.

DP7 (VQWRIRVAVIRK) is a cationic cell-penetrating peptide. Previous studies have demonstrated that cholesterol-modified DP7 exhibits reduced cytotoxicity and an enhanced safety profile in comparison to unmodified DP7.<sup>31</sup> Our previous study found that with the help of GalNAc, a kind of high affinity liver-targeting ligand, DP7-C led to an

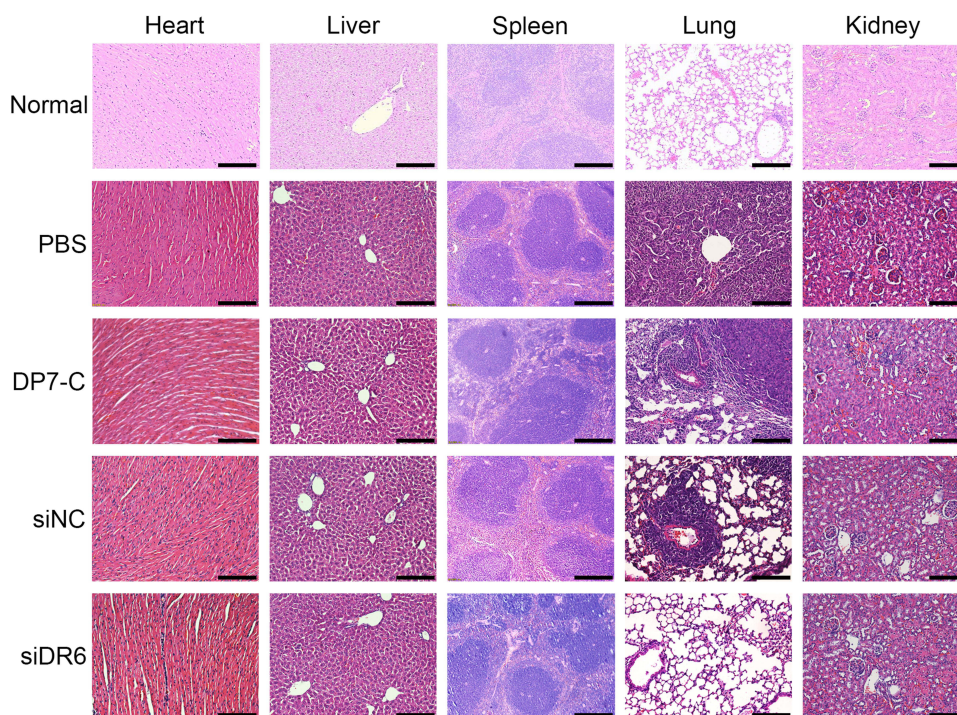


**Figure 7** Safety evaluation of DP7-C intravenous administration. HE analysis. Scar bar, 200µm.

enhancement in the transfection efficiency of GalNac-siRNA following its arrival in liver and promote the rapid escape of GalNac-siRNA in liver cells, which results in therapeutic effects on hepatocellular carcinoma.<sup>40</sup> In this study, it was found that DP7-C/siRNA could achieve efficient lung targeting in the absence of other targeting vectors, which may be attributed to the intravenous administration route used. Previous studies have indicated that many delivery vehicles such as liposomes, microparticles and nanoparticles possess the capacity to deliver drugs to lung tissue via intravenous injection.<sup>35</sup> A deeper underlying mechanism might involve particle size, as numerous studies have highlighted size as a key factor influencing lung targeting. A substantial body of research has demonstrated that micron-sized particles can be captured in the pulmonary capillaries, thereby facilitating lung accumulation.<sup>41–43</sup> Furthermore, researchers have demonstrated that certain nanoscale cationic carrier/siRNA complexes can aggregate into micron-sized particles in serum, which may contribute to passive lung targeting.<sup>44,45</sup> Given that DP7-C is also a cationic carrier and the size of DP7-C/siRNA complexes is in the nanoscale range, this may provide a rationale for the successful lung targeting observed after the intravenous administration of DP7-C/siRNA. Furthermore, DP7-C can deliver siRNA to both lung endothelial cells and lung tumor cells, which may offer a potential avenue for the treatment of lung cancer or metastatic lung cancer.

As a member of the tumor necrosis factor (TNF) family, DR6 is a promising target for antitumor therapy. Recent studies have demonstrated that DR6 is highly expressed in certain tumors.<sup>46,47</sup> Furthermore, knockdown of DR6 in tumor cells has been shown to affect tumor growth. The mechanism may be related to the fact that inhibition of DR6 expression can block the expression of IL-6 and thereby inhibit the activation of p-STAT3 and suppress the promotion of angiogenesis-related cytokine expression.<sup>19</sup> In the present study, we combined DP7-C and siDR6. Firstly, cholesterol-modified DP7 exhibited higher siRNA transfection efficiency and lower cytotoxicity than other commonly used transfection agents, such as PEI25K and Lipo2000. Secondly, intravenous injection of DP7-C/siRNA complexes resulted in efficient aggregation in the mouse lungs. Besides, DP7-C was demonstrated to be an effective delivery vehicle for siDR6, exhibiting high gene silencing efficiency. Furthermore, the suppression of DR6 expression was found to result in the inhibition of the IL-6/STAT3 pathway. Other studies have demonstrated that tumor cell-induced endothelial cell necrosis represents an important pathogenic mechanism underlying tumor metastasis.<sup>25</sup> Consequently, inhibition of tumor-induced endothelial cell necrosis may represent a promising strategy for the treatment of tumor lung metastasis.

It has been demonstrated that ligands for DR6 expressed on tumor cells can bind to DR6 on pulmonary vascular endothelial cells, resulting in endothelial cell necrosis and the subsequent triggering of tumor metastasis.<sup>25</sup> In this study, we successfully inhibited the expression of DR6 in lung endothelial cells and prevented the formation of metastatic lung cancer by intravenously injecting the DP7-C/siDR6 complex.

In addition, it has been proposed in the literature that the silencing of DR6 expression may result in a reduction in monocyte infiltration into the tumor microenvironment.<sup>47</sup> Our previous studies have demonstrated that DP7-C has an immunomodulatory effect, recruiting monocytes and macrophages.<sup>30</sup> Based on these findings, we conducted experiments to assess the recruitment of monocytes, macrophages, CD4<sup>+</sup> and CD8<sup>+</sup> T cells by DP7-C to the tumor microenvironment following intravenous injection, either alone or in combination with siRNA. The results demonstrated that the infiltration of immune cells into the tumor microenvironment was augmented in the DP7-C treatment group. However, there was no significant difference in tumor size between the DP7-C-treated group and the PBS group. This may be attributed to the relatively low dose of DP7-C administered, which was 60 µg per dose (approximately 3 mg/kg). This dose is considerably lower than the recommended safe dose (80 mg/kg), which may be indicative of the fact that, although DP7-C demonstrates immunomodulatory properties, it is insufficient to induce tumour inhibition. The experimental results obtained also demonstrate that, although DP7-C increased the infiltration of immune cells in the tumour in comparison with the PBS group, the level of infiltration was not as substantial as that observed with DP7-C/siDR6. This finding serves to further emphasise the significance of DP7-C in combination with siDR6 treatment. Furthermore, immune tolerance may occur at a later stage of treatment, which may explain the lack of antitumor effect observed with DP7-C alone. In the prophylactic B16F10 lung metastasis model, the DP7-C group demonstrated a therapeutic effect, although the difference was not statistically significant. Consequently, this may substantiate the role of immunomodulation in the initial stages of antitumor therapy.

The findings of this study indicate that DP7-C can be employed as a straightforward, efficacious, and secure siRNA transfection agent *in vitro* and *in vivo*. This study describes the mechanism of the anti-tumor effect of intravenous DP7-C/siDR6 in two main aspects. Firstly, the DP7-C/siDR6 complex silenced DR6 expressed in tumor cells. This silencing also affects the expression of vascular endothelial growth factor (VEGF) by influencing the IL-6/STAT3 pathway, thereby inhibiting tumor angiogenesis and impeding tumor growth. Secondly, the DP7-C/siDR6 complex exhibits high stability following intravenous administration, enabling successful silencing of DR6 expressed in lung endothelial cells. This, in turn, protects the endothelial cell barrier and prevents tumor metastasis.

However, despite the many advantages of the therapeutic strategy of systemic delivery of DP7-C micelles carrying siDR6, there are still some challenges to overcome. For example, how to go further to achieve precise targeting in the lungs but not in other tissues. How to further evaluate the long-term safety. How to achieve precise control of the shape and size of self-assembled peptide nanomaterials enables precise transport of biomimetic components with multiple biological functions as well as at the subcellular level.<sup>48</sup> These issues require further in-depth studies and research. In addition, we should also note that the safety and efficacy of gene therapy, as an emerging therapeutic tool, still requires further clinical validation. In future studies, we need to combine more data from clinical trials and animal experiments to comprehensively evaluate the effects and risks of the therapeutic strategy of systemic administration of DP7-C micelles carrying siDR6 in the treatment of metastatic lung cancer.

## Conclusion

Herein, the systemic delivery of DP7-C micelles carrying siDR6 for lung-targeted therapeutic strategies offers novel concepts and methodologies for the treatment of lung metastatic cancer. The preliminary results indicate that DP7-C can be used as a safe and effective carrier for systemic siRNA delivery. The DP7-C/siDR6 delivery system may serve as an alternative therapeutic approach for lung metastatic cancers, with the potential to produce good anti-tumor effects. Although there are still some challenges and problems that need to be solved, with the continuous advancement of technology and deeper research, there is reason to believe that this strategy will play an important role in the future treatment of lung cancer.

## Ethical Approval and Consent to Participate

All animal procedures were approved and controlled by the Institutional Animal Care and Treatment Committee of Sichuan University and conducted according to the Animal Care and Use Guidelines of Sichuan University.

## Author Contributions

All authors made a significant contribution to the work reported, whether that is in the conception, study design, execution, acquisition of data, analysis and interpretation, or in all these areas; took part in drafting, revising or critically reviewing the article; gave final approval of the version to be published; have agreed on the journal to which the article has been submitted; and agree to be accountable for all aspects of the work.

## Funding

This work was supported by the National Key Research and Development Program of China (No. 2023YFC3405200), the National Natural Science Foundation of China (No. 82471854, 82073366), the 1.3.5 project for disciplines of excellence, West China Hospital, Sichuan University (No. ZYGD23008) and the National Clinical Research Center for Geriatrics, West China Hospital, Sichuan University (Z2023JC002).

## Disclosure

Professor Li Yang reports a patent ZL20201110738.5 issued to West China Hospital of Sichuan University. The authors declare that they have no competing interests.

## References

1. Ganesh K, Massague J. Targeting metastatic cancer. *Nat Med.* 2021;27(1):34–44. doi:10.1038/s41591-020-01195-4
2. Wan L, Pantel K, Kang Y. Tumor metastasis: moving new biological insights into the clinic. *Nat Med.* 2013;19(11):1450–1464. doi:10.1038/nm.3391
3. Seyfried TNS, Huysentruyt LCTN. On the origin of cancer metastasis. *Crit Rev Oncog.* 2013;18(1–2):43–73. doi:10.1615/CritRevOncog.v18.i1-2.40
4. Chiesa AM, Spinnato P, Miceli M, Facchini G. Radiologic assessment of osteosarcoma lung metastases: state of the art and recent advances. *Cells.* 2021;10(3):553. doi:10.3390/cells10030553
5. Wu M, Liang Y, Zhang X. Changes in pulmonary microenvironment aids lung metastasis of breast cancer. *Front Oncol.* 2022;12:860932. doi:10.3389/fonc.2022.860932
6. Xiong K, Qi M, Stoeger T, Zhang J, Chen S. The role of tumor-associated macrophages and soluble mediators in pulmonary metastatic melanoma. *Front Immunol.* 2022;13:1000927. doi:10.3389/fimmu.2022.1000927
7. Xu R, Yan Y, Zheng X, et al. Aspirin suppresses breast cancer metastasis to lung by targeting anoikis resistance. *Carcinogenesis.* 2022;43(2):104–114. doi:10.1093/carcin/bgab117
8. Li J, Yuan Y, Yang F, et al. Expert consensus on multidisciplinary therapy of colorectal cancer with lung metastases (2019 edition). *J Hematol Oncol.* 2019;12(1):16. doi:10.1186/s13045-019-0702-0
9. Liu Y, Mao D, Wang H, Che X, Chen Y. Formation of pre-metastatic niches induced by tumor extracellular vesicles in lung metastasis. *Pharmacol Res.* 2023;188:106669. doi:10.1016/j.phrs.2023.106669
10. Hirano H, Boku N. The current status of multimodality treatment for unresectable locally advanced esophageal squamous cell carcinoma. *Asia Pac J Clin Oncol.* 2018;14(4):291–299. doi:10.1111/ajco.12995
11. Wang J, Wu M, Zheng D, et al. Garcinol inhibits esophageal cancer metastasis by suppressing the p300 and TGF-beta1 signaling pathways. *Acta Pharmacol Sin.* 2020;41(1):82–92. doi:10.1038/s41401-019-0271-3
12. Kakeji Y, Oshikiri T, Takiguchi G, et al. Multimodality approaches to control esophageal cancer: development of chemoradiotherapy, chemotherapy, and immunotherapy. *Esophagus.* 2021;18(1):25–32. doi:10.1007/s10388-020-00782-1
13. Yuan M, Zhang X, Zhang J, et al. DC-SIGN-LEF1/TCF1-miR-185 feedback loop promotes colorectal cancer invasion and metastasis. *Cell Death Differ.* 2020;27(1):379–395. doi:10.1038/s41418-019-0361-2
14. Fares J, Fares MY, Khachfe HH, Salhab HA, Fares Y. Molecular principles of metastasis: a hallmark of cancer revisited. *Signal Transduct Target Ther.* 2020;5(1):28. doi:10.1038/s41392-020-0134-x
15. Lin Y, Xu J, Lan H. Tumor-associated macrophages in tumor metastasis: biological roles and clinical therapeutic applications. *J Hematol Oncol.* 2019;12(1):76. doi:10.1186/s13045-019-0760-3
16. Wong KM, Song J, Saini V, Wong YH. Small molecules as drugs to upregulate metastasis suppressors in cancer cells. *Curr Med Chem.* 2019;26(32):5876–5899. doi:10.2174/0929867325666180522090842
17. Peinado H, Zhang H, Matei IR, et al. Pre-metastatic niches: organ-specific homes for metastases. *Nat Rev Cancer.* 2017;17(5):302–317. doi:10.1038/nrc.2017.6
18. Carpinteiro A, Becker KA, Japtok L, et al. Regulation of hematogenous tumor metastasis by acid sphingomyelinase. *EMBO Mol Med.* 2015;7(6):714–734. doi:10.15252/emmm.201404571

19. Yang X, Shi B, Li L, et al. Death receptor 6 (DR6) is required for mouse B16 tumor angiogenesis via the NF-kappaB, P38 MAPK and STAT3 pathways. *Oncogenesis*. 2016;5(3):e206. doi:10.1038/oncsis.2016.9
20. R B, T W, S N. Tumor necrosis factor receptor superfamily member 21:TNFR-related death receptor-6, DR6. *Adv Exp Med Biol*. 2009;647:186–194. doi:10.1007/978-0-387-89520-8\_13
21. Pan G, Bauer JH, Haridas V, et al. Identification and functional characterization of DR6, a novel death domain-containing TNF receptor. *FEBS Lett*. 1998;431(3):351–356. doi:10.1016/s0014-5793(98)00791-1
22. K GM, Jj. L, D. L, et al. Tumor necrosis factor- $\alpha$  induces the expression of DR6, a member of the TNF receptor family, through activation of NF-kB. *Oncogene*. 2001;20:7965–7975. doi:10.1038/sj.onc.1204985
23. Kuester M, Kemmerzehl S, Dahms SO, Roeser D, Than ME. The crystal structure of death receptor 6 (DR6): a potential receptor of the amyloid precursor protein (APP). *J Mol Biol*. 2011;409(2):189–201. doi:10.1016/j.jmb.2011.03.048
24. Nikolaev A, McLaughlin T, O'Leary DD, Tessier-Lavigne M. APP binds DR6 to trigger axon pruning and neuron death via distinct caspases. *Nature*. 2009;457(7232):981–989. doi:10.1038/nature07767
25. Strilic B, Yang L, Albarran-Juarez J, et al. Tumour-cell-induced endothelial cell necroptosis via death receptor 6 promotes metastasis. *Nature*. 2016;536(7615):215–218. doi:10.1038/nature19076
26. Ramos-Gonzalez MR, Vazquez-Garza E, Garcia-Rivas G, Rodriguez-Aguayo C, Chavez-Reyes A. Therapeutic effects of WT1 silencing via respiratory administration of neutral DOPC liposomal-siRNA in a lung metastasis melanoma murine model. *Noncoding RNA*. 2023;9(2). doi:10.3390/ncrna9020021
27. Mainini F, Eccles MR. Lipid and polymer-based nanoparticle siRNA delivery systems for cancer therapy. *Molecules*. 2020;25(11):2692. doi:10.3390/molecules25112692
28. Ma Z, Wong SW, Forgham H, et al. Aerosol delivery of star polymer-siRNA nanoparticles as a therapeutic strategy to inhibit lung tumor growth. *Biomaterials*. 2022;285:121539. doi:10.1016/j.biomaterials.2022.121539
29. Zhang J, Chen B, Gan C, Sun H, Zhang J, Feng L. A comprehensive review of small interfering RNAs (siRNAs): mechanism, therapeutic targets, and delivery strategies for cancer therapy. *Int J Nanomed*. 2023;18:7605–7635. doi:10.2147/IJN.S436038
30. Zhang R, Tang L, Tian Y, et al. Cholesterol-modified DP7 enhances the effect of individualized cancer immunotherapy based on neoantigens. *Biomaterials*. 2020;241:119852. doi:10.1016/j.biomaterials.2020.119852
31. Zhang R, Wu F, Wu L, et al. Novel self-assembled micelles based on cholesterol-modified antimicrobial peptide (DP7) for safe and effective systemic administration in animal models of bacterial infection. *Antimicrob Agents Chemother*. 2018;62(11):e00368–18. doi:10.1128/aac
32. Biswas A, Chakraborty K, Dutta C, et al. Engineered histidine-enriched facial lipopeptides for enhanced intracellular delivery of functional siRNA to triple negative breast cancer cells. *ACS Appl Mater Interfaces*. 2019;11(5):4719–4736. doi:10.1021/acsami.8b13794
33. Hammond SM, Aartsma-Rus A, Alves S, et al. Delivery of oligonucleotide-based therapeutics: challenges and opportunities. *EMBO Mol Med*. 2021;13(4):e13243. doi:10.15252/emmm.202013243
34. Yi A, Sim D, Lee YJ, Sarangthem V, Park RW. Development of elastin-like polypeptide for targeted specific gene delivery in vivo. *J Nanobiotechnol*. 2020;18(1):15. doi:10.1186/s12951-020-0574-z
35. Wei Y, Zhao L. Passive lung-targeted drug delivery systems via intravenous administration. *Pharm Dev Technol*. 2014;19(2):129–136. doi:10.3109/10837450.2012.757782
36. Zhang R, Tang L, Tian Y, et al. DP7-C-modified liposomes enhance immune responses and the antitumor effect of a neoantigen-based mRNA vaccine. *J Control Release*. 2020;328:210–221. doi:10.1016/j.jconrel.2020.08.023
37. Yang CH, Fan M, Slominski AT, Yue J, Pfeffer LM. The role of constitutively activated STAT3 in B16 melanoma cells. *Int J Interferon Cytokine Mediat Res*. 2010;2010(2):1–7. doi:10.2147/IJICMR.S6657
38. Zou S, Tong Q, Liu B, Huang W, Tian Y, Fu X. Targeting STAT3 in Cancer Immunotherapy. *mol Cancer*. 2020;19(1):145. doi:10.1186/s12943-020-01258-7
39. Zhang R, Tang L, Zhao B, et al. A peptide-based small RNA delivery system to suppress tumor growth by remodeling the tumor microenvironment. *Mol Pharm*. 2021;18(3):1431–1443. doi:10.1021/acs.molpharmaceut.0c01253
40. Zhao B, Zhou B, Shi K, et al. Sustained and targeted delivery of siRNA/DP7-C nanoparticles from injectable thermosensitive hydrogel for hepatocellular carcinoma therapy. *Cancer Science*. 2021;112(6):2481–2492. doi:10.1111/cas.14903
41. Sahin S, Selek H, Ponchel G, et al. Preparation, characterization and in vivo distribution of terbutaline sulfate loaded albumin microspheres. *J Control Release*. 2002;82(2–3):345–358. doi:10.1016/S0168-3659(02)00141-4
42. Kutscher HL, Chao P, Deshmukh M, et al. Enhanced passive pulmonary targeting and retention of PEGylated rigid microparticles in rats. *Int J Pharm*. 2010;402(1–2):64–71. doi:10.1016/j.ijpharm.2010.09.020
43. Fang CL, Wen CJ, Aljuffali IA, Sung CT, Huang CL, Fang JY. Passive targeting of phosphatidylserine increases rolipram delivery to the lungs for treatment of acute lung injury: an animal study. *J Control Release*. 2015;213:69–78. doi:10.1016/j.jconrel.2015.06.038
44. Han J, Wang Q, Zhang Z, Gong T, Sun X. Cationic bovine serum albumin based self-assembled nanoparticles as siRNA delivery vector for treating lung metastatic cancer. *Small*. 2014;10(3):524–535. doi:10.1002/sml.201301992
45. Kim J, Jeon S, Kang SJ, et al. Lung-targeted delivery of TGF- $\beta$  antisense oligonucleotides to treat pulmonary fibrosis. *J Control Release*. 2020;322:108–121. doi:10.1016/j.jconrel.2020.03.016
46. Jia J, Huang Y, Chen Q, et al. DR6 augments colorectal cancer cell growth, invasion, and stemness by activating AKT/NF-kappaB pathway. *Biochem Genet*. 2024. doi:10.1007/s10528-024-10673-0
47. Ren X, Lin Z, Yuan W. A structural and functional perspective of death receptor 6. *Front Pharmacol*. 2022;13:836614. doi:10.3389/fphar.2022.836614
48. Wang Y, Zhan J, Huang J, et al. Dynamic responsiveness of self-assembling peptide-based nano-drug systems. *Interdisciplin Med*. 2023;1(1). doi:10.1002/inmd.20220005

**International Journal of Nanomedicine**

**Dovepress**

Taylor & Francis Group

## **Publish your work in this journal**

The International Journal of Nanomedicine is an international, peer-reviewed journal focusing on the application of nanotechnology in diagnostics, therapeutics, and drug delivery systems throughout the biomedical field. This journal is indexed on PubMed Central, MedLine, CAS, SciSearch<sup>®</sup>, Current Contents<sup>®</sup>/Clinical Medicine, Journal Citation Reports/Science Edition, EMBase, Scopus and the Elsevier Bibliographic databases. The manuscript management system is completely online and includes a very quick and fair peer-review system, which is all easy to use. Visit <http://www.dovepress.com/testimonials.php> to read real quotes from published authors.

Submit your manuscript here: <https://www.dovepress.com/international-journal-of-nanomedicine-journal>